RSC Advances

PAPER

View Article Online
View Journal | View Issue

Cite this: *RSC Adv.*, 2019, **9**, 35717

Structure and luminescence properties of multicolor phosphor $Ba_2La_3(GeO_4)_3F:Tb^{3+},Eu^{3+}$†

Xiaoxue Ma,[a] Libing Liao, *[a] Qingfeng Guo, [b] Haikun Liu,[a] Dan Yang,[a] Ning Liu[a] and Lefu Mei*[a]

Received 30th July 2019
Accepted 28th October 2019

DOI: 10.1039/c9ra05915f

rsc.li/rsc-advances

A new kind of multicolor phosphor $Ba_2La_3(GeO_4)_3F:0.15Tb^{3+},xEu^{3+}$ (BLGOF:$0.15Tb^{3+},xEu^{3+}$) has been acquired through the traditional high temperature solid phase synthesis method. The structural information of the phosphor was studied by X-ray diffraction (XRD), scanning electron microscopy (SEM) and Rietveld refinement. The optical properties of the phosphor have also been studied in detail, including its photoluminescence spectra (PL), photoluminescence excitation spectra (PLE), fluorescence decay curves, energy transfer mechanism and thermal quenching spectra. It has been found that the optimum concentration of Eu^{3+} in BLGOF:$0.15Tb^{3+},xEu^{3+}$ is 0.24 mol and the energy transfer mechanism from Tb^{3+} to Eu^{3+} in BLGOF is quadrupole–quadrupole. The color of BLGOF:$0.15Tb^{3+},xEu^{3+}$ phosphors can be changed from green to yellow/orange to red. Some details of the energy transfer are reviewed and the effect of complex anion regulation on thermal stability has also been studied. All the properties are good and can contribute to the promotion from the laboratory to practical application for the phosphor.

1. Introduction

The lighting industry has a huge impact on the development of human society. In a long history, the lighting industry has undergone many updates. At present, the most popular lighting fixtures are light-emitting diodes (LEDs), among which white LEDs are known as the fourth-generation lighting source.[1–4] White LEDs (w-LEDs) have many advantages, such as environmental protection, pollution-free, energy saving, low carbon, long service life, low starting voltage, high brightness and so on. So many advantages make w-LEDs widely used, including in the exhibition industry, advertising industry, municipal lighting and even general lighting. Due to the reasons above, w-LEDs have also been a research hotspot in scientific research in recent years.[5–8]

During the illumination of w-LEDs, chips would be used to excite phosphors to obtain white light with practical application value.[9–11] The method of obtaining white light *via* mixing multicolor phosphors was popular in recent years. Phosphors consist of host and activators and activators are usually rare earth ions or variable metal ions. One of the common methods for obtaining single-phase multicolor phosphors is energy transfer, *i.e.* fixing the concentration of energy transfer ion to the sensitizer and changing the concentration of activator to obtain multicolor phosphors, and $Tb^{3+} \rightarrow Eu^{3+}$ ion pair is widely used.[12–15] As for the host, the apatite structure compounds have been extensively developed because of their advantages such as rich crystal field environment, structural stability, and so on. The chemical expression of natural apatite is $Ca_5(PO_4)_3F$ and the apatite structure compounds can be expressed as $M_{10}(XO_4)_6Y_2$, in which M usually stands for Ca, Ba, Sr, Mn, *etc.*; X usually stands for Si, Ge, P, *etc.*; Y usually stands for F, Cl, Br, O, *etc.*[16–19] It can be inferred from the formula that the apatite structure compounds are available in many combinations based on the isomorphism and solid solution methods. Rich host structures could provide a large library of materials for the lighting industry. However, there is no report about the apatite structure phosphor of $Ba_2La_3(GeO_4)_3F:Tb^{3+},Eu^{3+}$ to best of our knowledge.

In this report, the research on the new multicolor phosphor BLGOF:Tb^{3+},Eu^{3+} has been focused on the structure and luminescence properties. The structure information of the phosphor was studied by XRD, SEM and Rietveld refinement. The optical properties of the phosphor have also been studied in detail, including PL, PLE, fluorescence quenching mechanism, thermal spectra, fluorescence lifetime and so on. All the properties are good enough and could contribute to the practical application for this phosphor.

[a]*Beijing Key Laboratory of Materials Utilization of Nonmetallic Minerals and Solid Wastes, National Laboratory of Mineral Materials, School of Materials Science and Technology, China University of Geosciences, Beijing 100083, China. E-mail: clayl@cugb.edu.cn; mlf@cugb.edu.cn; Fax: +86-10-82322974; +86-10-8232-1701; Tel: +86-10-82322039; +86-10-8233-1701*

[b]*School of Gemmology, China University of Geosciences, Beijing 100083, China*

† Electronic supplementary information (ESI) available. See DOI: 10.1039/c9ra05915f

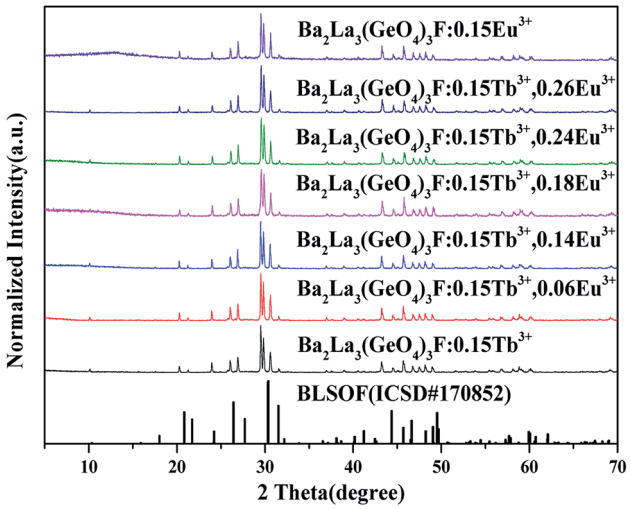

Fig. 1 XRD patterns of BLGOF:0.15Tb^{3+}, BLGOF:0.15Eu^{3+}, BLGOF:0.15Tb^{3+},xEu^{3+} (x = 0.06, 0.14, 0.18, 0.24, and 0.26) phosphors, and standard data of BLSOF (ICSD#170852) is shown as a reference.

2. Experimental details

2.1 Synthesis

Conventional solid-state method under high temperature was used to prepare the aimed phosphors BLGOF:Tb^{3+},Eu^{3+}. The raw materials were $BaCO_3$ (Beijing Chemical Pharmaceutical Factory, A.R.), La_2O_3 (China Pharmaceutical Group Pharmaceutical Co., Ltd., 99.99%), GeO_2 (China Pharmaceutical Group Pharmaceutical Co., Ltd., 99.99%), NH_4F (Beijing Chemical Pharmaceutical Factory, A.R.), Tb_4O_7 (99.99%) and Eu_2O_3 (99.99%) and were used directly without processing. The selected starting materials were weighed by the electronic balance with 0.0001 g accuracy according to stoichiometric ratio. Afterwards they were mixed into an agate mortar and grounded thoroughly. Then the stoichiometric mixture was transferred into an alumina crucible and the crucible was sealed into a high temperature tube furnace and annealed at 1350 °C for 4 h. At last, the sample was cooled to room temperature gradually and ground into powder again for a series of tests followed.

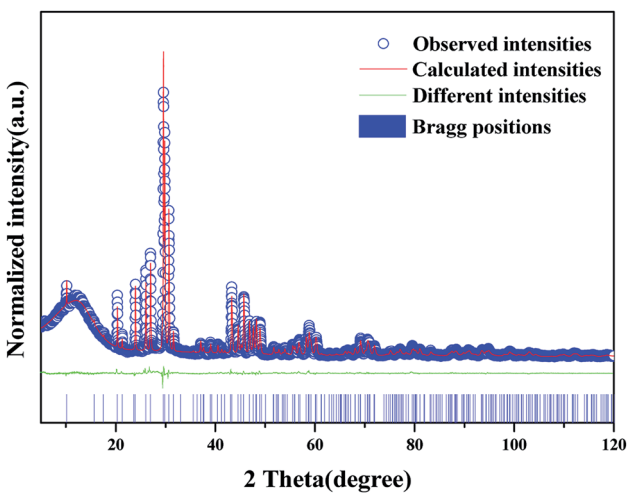

Fig. 2 Structure refinement of BLGOF (the red solid line, blue circles, short blue verticals and green solid lines represent the calculated pattern, the observed pattern obtained from XRD measurements, the Bragg positions, and the difference between the observed and calculated patterns, respectively).

Table 1 Refinement parameters for $Ba_2La_3(GeO_4)_3F$ obtained from the Rietveld refinement using X-ray powder diffraction data at room temperature

Formula	$Ba_2La_3(GeO_4)_3F$
Space group	$P6_3/m$
Crystal system	Hexagonal
a/b (nm)	1.0157(18)
c (nm)	0.7464(14)
a/b	90°
γ	120°
V (nm^3)	0.6668(26)
R-Bragg	3.54169787
R_{exp} (%)	4.548
R_{wp} (%)	6.259
R_p (%)	4.830
χ^2	1.375

2.2 Measurement

2.2.1 Structure and morphology. XRD patterns to determine the structure type were obtained *via* an X-ray powder diffractometer (D8 Advance, Bruker, Germany) with Cu-Kα radiation (λ = 0.15406 nm) operated at 40 kV and 30 mA. Powder diffraction data were fitted to obtain cell parameters by the Rietveld method using the computer software TOPAS 3.0 package.[20] Morphology, element distribution and composition of the compounds were observed by the method of SEM (JSM-6701F, Hitachi, Japan) with the accelerating voltage of 15 kV. The powder was attached to the conducting resin directly and sprayed with nano-platinum on the surface. The quantum efficiency of $Ba_2La_3(GeO_4)_3F$:0.15Tb^{3+},0.24Eu^{3+} sample was measured on a UV-vis-NIR spectrophotometer (UV-365).

Table 2 Fractional atomic coordinates, and occupancies parameters of BLGOF obtained from the Topas Rietveld Refinement using X-ray powder diffraction data at room temperature

Atom	x	y	z	occ	beq
La_2	0.24324(22)	0.98660(28)	0.25	0.55	1
Ba_2	0.24324(20)	0.98660(28)	0.25	0.45	1
La_1	0.6666667	0.3333333	0.99794(55)	0.55	1
Ba_1	0.6666667	0.3333333	0.99794(55)	0.45	1
Ge_1	0.40454(36)	0.37250(34)	0.25	1	1
O_1	0.5974	0.4496	0.25	1	1
O_2	0.3442	0.4996	0.25	1	1
O_3	0.3560	0.2721	0.0751	1	1
F	0	0	0.25	1	2.81

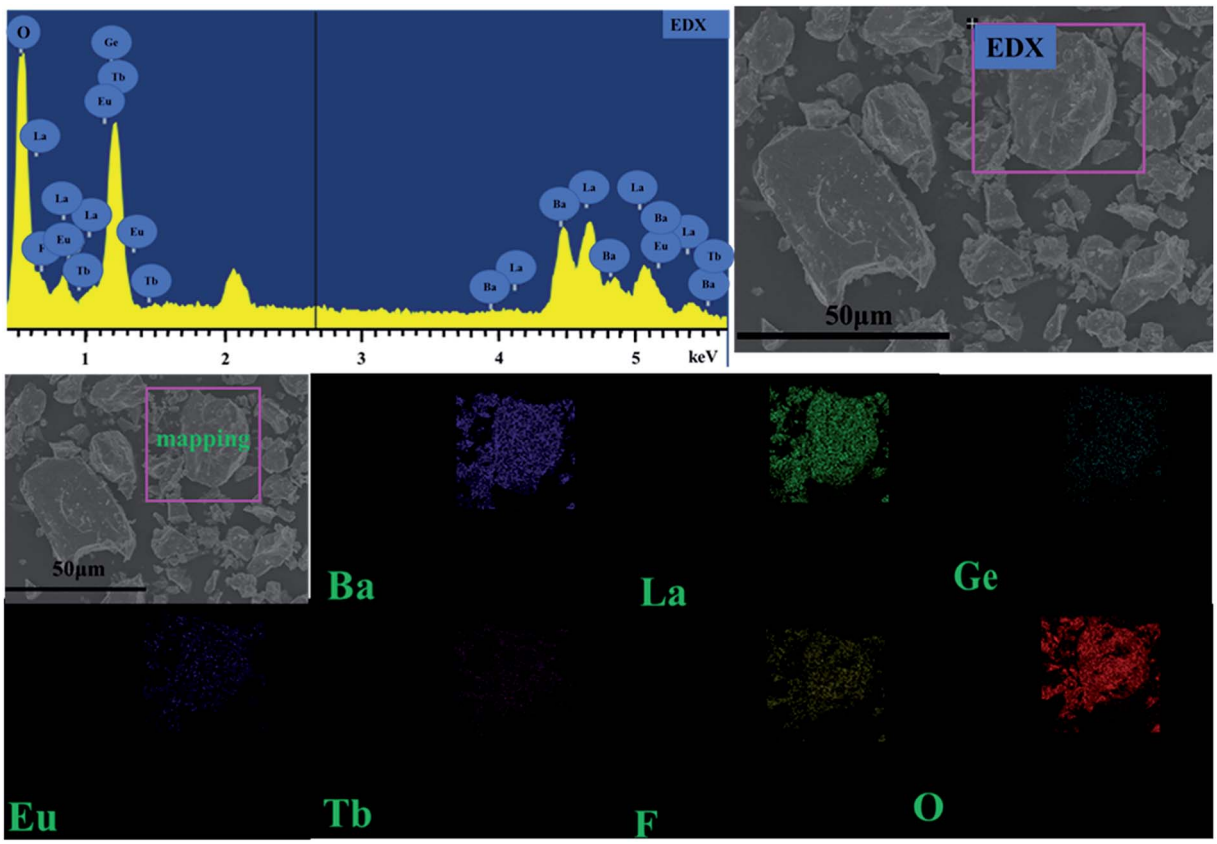

Fig. 3 (Top right) SEM image of BLGOF:0.15Tb^{3+},0.15Eu^{3+} phosphor (Top left) EDX spectra of BLGOF:0.15Tb^{3+},0.15Eu^{3+} phosphors (Bottom) elemental distribution of BLGOF:0.15Tb^{3+},0.15Eu^{3+} phosphors.

2.2.2 Spectra. Excitation and emission spectra under room temperature were characterized on a Hitachi F-4600 fluorescence spectrophotometer. Photoluminescence (PL) system equipped with a xenon lamp (400 V, 150 W) acted as an excitation source. The 400 nm cut off filter was applied in the experiment to clear up the second-order emission of source radiation. Thermal spectra were measured on the same spectrophotometer, which was combined with a self-made heating attachment and a computer-controlled electric furnace. Decay curves were monitored by an Edinburgh FS5 Combined Fluorescence Lifetime & Steady State Spectrometer.

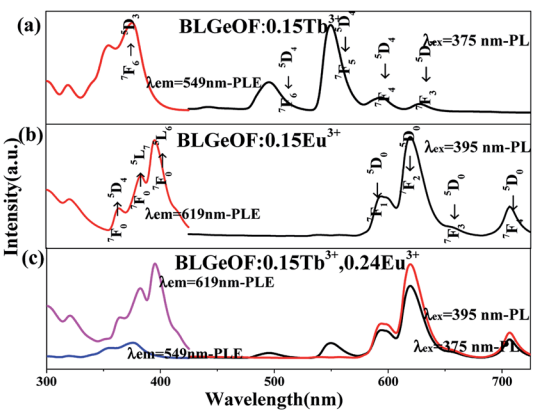

Fig. 4 (a) PLE spectrum (left) and PL spectrum (right) of BLGOF:0.15Tb^{3+} (λ_{em} = 549 nm and λ_{ex} = 375 nm) (b) PLE (left) and PL (right) spectra of BLGOF:0.15Eu^{3+} (λ_{em} = 619 nm and λ_{ex} = 395 nm) (c) PLE (left) and PL (right) spectra of BLGOF:0.15Tb^{3+},0.22Eu^{3+}(λ_{em} = 619 nm and 549 nm; λ_{ex} = 375, and 395 nm).

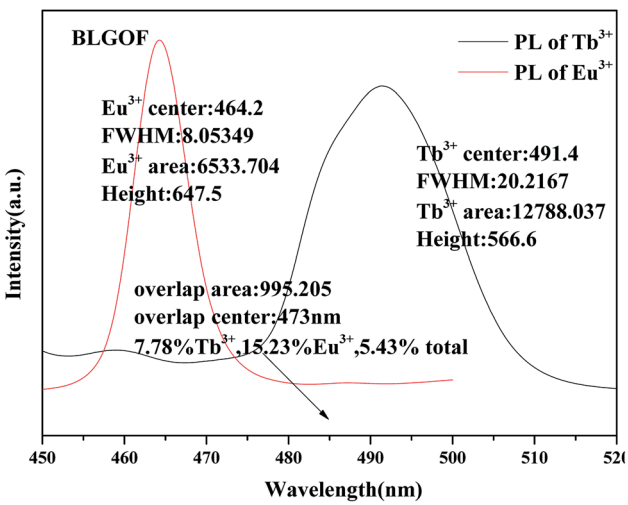

Fig. 5 Area integral and related parameters for the emission spectra of BLGOF:0.15Tb^{3+} phosphors, the excitation spectra of BLGOF:0.15Eu^{3+} phosphors and their overlapping parts.

3. Results and discussions

The XRD patterns of the synthetic samples were shown in Fig. 1. It is obvious that the XRD patterns of BLGOF:0.15Tb^{3+},xEu^{3+} phosphors can be accurately assigned to the phase of $Ba_2La_3(SiO_4)_3F$ (ICSD no. 170852, apatite, hexagonal, $p6_3/m$).[21] Only when the isomorphic replacement of Tb^{3+} and Eu^{3+} to La^{3+} atoms was successful in the present sample structure can these positions and intensities of diffraction peaks match well with the reference ICSD file. In addition, the diffraction peaks of the samples shifted to the smaller 2θ angle side (bigger d-spacing, *i.e.*, interplanar distances), which can be ascribed to the substitution of Si^{4+} by bigger Ge^{4+}. Therefore, according to the theory of isomorphism, it could be inferred that the doping which was caused by Tb^{3+} and Eu^{3+} did not cause the structural change.[22–25]

To further understand the crystallographic information of the synthesized samples, powder diffraction data were fitted by the Rietveld method and the results are presented in Fig. 2, Tables 1 and 2. The observed (blue circles), calculated (red line), and difference (green line) XRD profiles shown in Fig. 2 are the Rietveld refinement of BLGOF at 298 K with $\lambda = 1.5406$ Å. Crystal structure of $Ba_2La_3(SiO_4)_3F$ (apatite-type structure) was taken as starting model for Rietveld refinement. All the experimental peaks are well fitted by the refinement, indicating that all of those peaks are Bragg reflections from the BLGOF structure and converge to $R_{exp} = 4.548\%$, $R_{wp} = 6.259\%$, $R_p = 4.830\%$ and $\chi^2 = 1.375$. As can be seen from Table 1, the refinement is stable and gives low R-factors. In the BLGOF compound, the lattice parameters are determined to be $a = b = 1.0157$ nm, $c = 0.7464$ nm and $V = 0.6668$ nm^3, respectively. Moreover, the refined atomic positions and isotropic temperature factors for all atoms are listed in Table 2.[26,27]

In order to study the effect of structure regulation on crystal structure, we synthesized $Ba_2La_3(SiO_4)_1(GeO_4)_2F$ ($BLSi_1Ge_2F$) and $Ba_2La_3(SiO_4)_2(GeO_4)_1F$ ($BLSi_2Ge_1F$) hosts and refined their

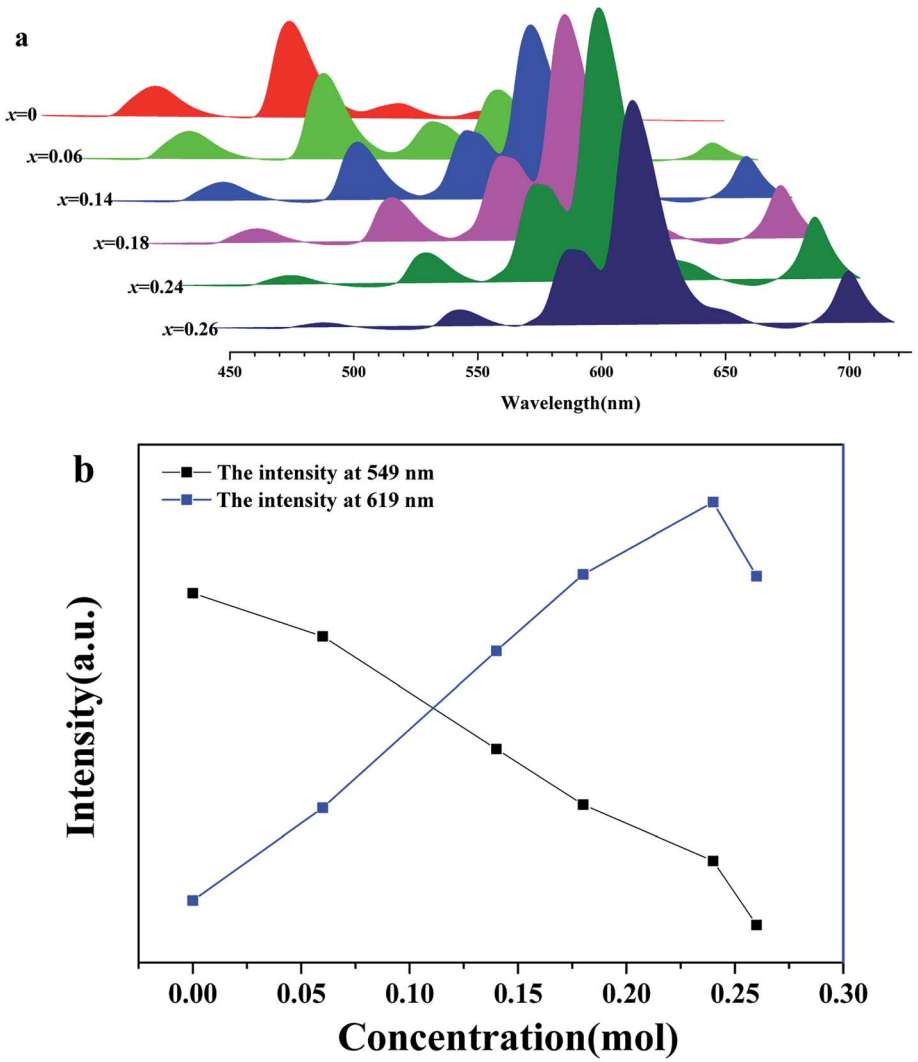

Fig. 6 (a) A series of luminescence spectra under 375 nm near-ultraviolet excitation of BLSOF:0.15Tb^{3+},xEu^{3+} ($x = 0$, 0.06, 0.14, 0.18, 0.24 and 0.26) (b) the emission intensities of 549 nm (Tb^{3+} characteristic emission spectra) and 619 nm (Eu^{3+} characteristic emission spectra) at different Eu^{3+} doping concentrations (x) were measured under 375 nm excitation.

structures. Tables S1 and S2† are the atomic coordinate information of $BLSi_1Ge_2F$ and $BLSi_2Ge_1F$. The cell parameters of several hosts are compared in Table S3.† Table S3† shows that the cell parameters increase with the increase of atomic radius. The structure control of complex anions can have a significant impact on the crystal structure, which may affect the properties of light emitting, energy transfer, thermal stability and so on.

To be more intuitive, the microstructure of BLGOF:0.15T-b^{3+},0.15Eu^{3+} was discovered by means of SEM and shown in the top right of Fig. 3. The sample composition seems to be irregular granules. The observation of Ba, La, Ge, O, F, Tb, Eu peaks in the EDX spectrum further implied the formation of the sample. In addition, the elemental mapping results as shown in the bottom of Fig. 3 demonstrated that all the elements in the sample were homogenously distributed over the granules.[28–30]

The optical properties of the phosphors were studied then. The PLE and PL spectra of BLGOF:0.15Tb^{3+}, BLGOF:0.15Eu^{3+} and BLGOF:0.15Tb^{3+},0.24Eu^{3+} were depicted in Fig. 4. It could be seen that the Fig. 4(a) were the luminescence spectra of BLGOF:0.15Tb^{3+} phosphor. The PLE spectra of BLGOF:0.15Tb^{3+} showed typical 325–500 nm excitation peaks of Tb^{3+} with characteristic excitation peak at 375 nm ($^7F_6 \rightarrow {}^5D_3$). Under 375 nm excitation, Tb^{3+} emission peaks at 491, 549, 592 and 624 nm with $^5D_4 \rightarrow {}^7F_J$ ($J = 6, 5, 4, 3$) transition as the core were observed.[31] Fig. 4(b) were the spectra of BLGOF:0.15Eu^{3+} phosphor. There were several peaks in the excitation spectra, which could be attributed to the transition of Eu^{3+} from the ground state $^7F_0$ to the excited state $^5D_4$ (362 nm), $^5L_7$ (381 nm), $^5L_6$ (395 nm), $^5D_3$ (414 nm) and $^5D_2$ (464 nm), respectively. Under 395 nm excitation, BLGOF:0.15Eu^{3+} phosphors emitted characteristic peaks of Eu^{3+} centered at 591 nm ($^5D_0 \rightarrow {}^7F_1$), 619 nm ($^5D_0 \rightarrow {}^7F_2$), and 654 and 700 nm originating from the $^5D_0 \rightarrow {}^7F_J$ ($J = 3$, 4) transition of Eu^{3+}. The excitation spectra of Eu^{3+} and the emission spectra of Tb^{3+} had a overlap, indicating that energy transfer from Tb^{3+} to Eu^{3+} could be realized.

Fig. 4(c) were the spectra of BLGOF:0.15Tb^{3+},0.24Eu^{3+} phosphors. In the same wavelength range, the PL spectra of 375 and 395 nm and the PLE spectra monitored by 549 and 619 nm were measured, and the relative intensities of Tb^{3+} and Eu^{3+} emission spectra and excitation spectra were compared. When 375 nm was used as excitation wavelength to excite the phosphor, the emission peaks of Eu^{3+} at 619 nm and Tb^{3+} at 549 nm could be observed, especially the emission peaks of Eu^{3+}, which indicated that the BLGOF single-phase phosphor co-doped with Tb^{3+}, Eu^{3+} could be adjusted from green to yellow, orange to red. When excited by 395 nm, only the characteristic peaks of Eu^{3+} could be observed. The 619 nm peak of the red spectrum is higher than that of the black one, which indicates that the emission intensity of Eu^{3+} decreases when the phosphor is excited by 375 nm wavelength. The emission spectra excited by 375 nm include not only the characteristic emission peaks of Eu^{3+} ($^5D_0$–$^7F_2$ at 619 nm), but also the characteristic emission peaks of Tb^{3+} ($^5D_4$–$^7F_{6,5}$). Therefore, in order to study the energy transfer from Tb^{3+} to Eu^{3+}, we focus on the spectral characteristics of 375 nm excitation.[32]

The overlapping part of emission spectrum (black, peak at 491 nm) of Tb^{3+} and excitation spectrum (red, peak at 464 nm) of Eu^{3+} was amplified as shown in Fig. 5. Using origin 9.0, the emission peaks of Tb^{3+} and the excitation peaks of Eu^{3+} and their overlaps are integrated respectively. The peak heights, half-width (FWHM) and peak areas are obtained as shown in the figure. Overlapping area accounts for 7.78% of Tb^{3+} emission peak area, 15.23% of Eu^{3+} excitation peak area, and the sum of Tb^{3+} emission peak area and Eu^{3+} excitation peak area decreases from 6.73% (BLSOF) to 5.43% (BLGOF). This overlap further proves the theoretical feasibility of energy transfer. The overlap area is smaller than that of BLSOF in terms of Tb^{3+} emission peak area and Eu^{3+} excitation peak area. This change may affect the energy transfer between Tb^{3+} and Eu^{3+}.[33]

Fig. 6(a) shows a series of emission spectra of BLGOF:0.15Tb^{3+},xEu^{3+} (x = 0, 0.06, 0.14, 0.18, 0.24 and 0.26) under near-ultraviolet excitation at 375 nm. The emission intensities of Tb^{3+} (549 nm) and Eu^{3+} (619 nm) at different concentrations (x) were shown in Fig. 6(b). It can be seen from

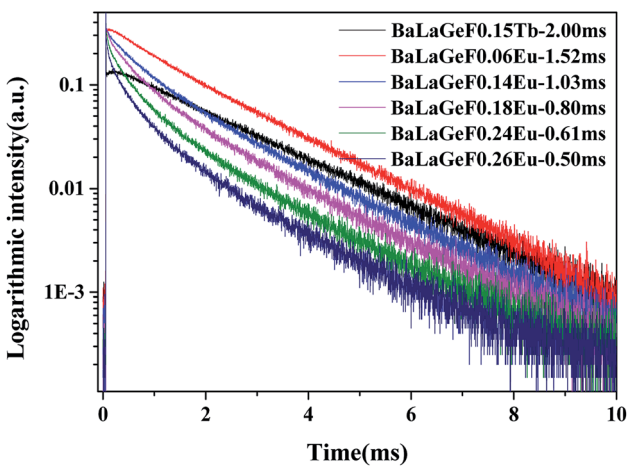

Fig. 7 The decay curves of BLGOF:0.15Tb^{3+},xEu^{3+} (x = 0, 0.06, 0.14, 0.18, 0.24, and 0.26) when excited by 375 nm and monitored by 549 nm.

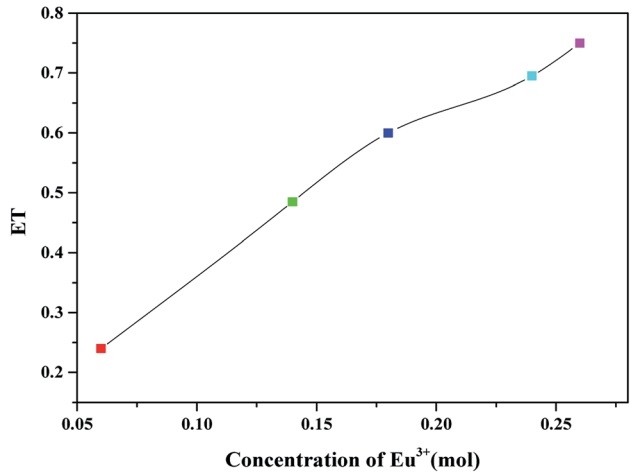

Fig. 8 The energy transfer efficiency from Tb^{3+} to Eu^{3+} of BLGOF:0.15Tb^{3+},xEu^{3+} (x = 0.06, 0.14, 0.18, 0.24, and 0.26) phosphors.

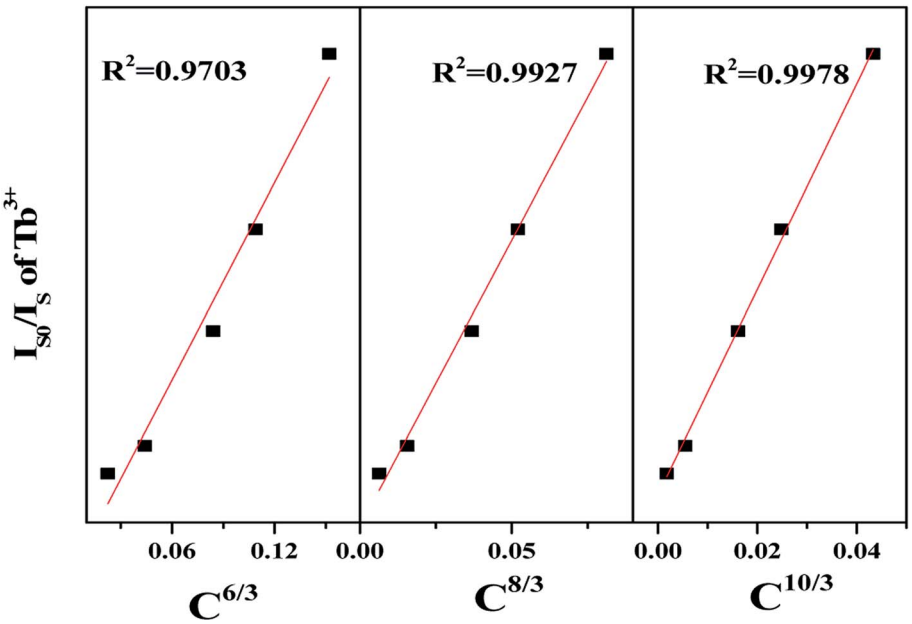

Fig. 9 The energy transfer mechanism from Tb^{3+} to Eu^{3+} of BLGOF:0.15Tb^{3+},xEu^{3+} (x = 0.06, 0.14, 0.18, 0.24, and 0.26) phosphors.

the figure that the emission intensity of Tb^{3+} (549 nm) decreases with the increasing doping concentration of Eu^{3+} (619 nm). This may be due to the fact that Tb^{3+} transmits part of its energy to Eu^{3+}. The emission intensity of Eu^{3+} (619 nm) increases first, and reaches the maximum when the doping concentration x = 0.24, then decreases. Concentration quenching may be responsible for the decrease of emission intensity of Eu^{3+} above x = 0.24. It can be inferred that energy transfer occurs from Tb^{3+} to Eu^{3+} in BLSOF.[34,35]

Fig. 7 mainly describes the decay curves of BLGOF:0.15Tb^{3+},xEu^{3+} excited by the light of 375 nm. The decay curve can be fitted perfectly based on the following decay equation as shown in the figure:[36]

$$I(t) = I_0 + A\exp(-t/\tau) \quad (1)$$

For the equation, I and I_0 stand the luminescence intensity at time t and 0, A is constant, t is the time, and τ is the decay time for the sample. Monitor wavelength of BLGOF:0.15Tb^{3+},xEu^{3+} decay curves is 549 nm, excitation wavelength is 375 nm. Obviously, the lifetime of Tb^{3+} decreases with the increase of Eu^{3+} concentration, which further confirms the energy transfer from Tb^{3+} to Eu^{3+} in BLGOF.

The energy transfer efficiency from Tb^{3+} to Eu^{3+} can be calculated by formula (2):[37,38]

$$\eta = 1 - (\tau_s/\tau_{s0}) \quad (2)$$

As shown in Fig. 8, when Eu^{3+} concentration is 0.06, 0.14, 0.18, 0.24 and 0.26 mol, the energy transfer efficiency is 24%, 48.5%, 60%, 69.5% and 75%, respectively. As the concentration of Eu^{3+} increases, the energy transfer efficiency increases.

Based on BLASSE theory, the critical distance R_c can be calculated by formula (3)[39,40]

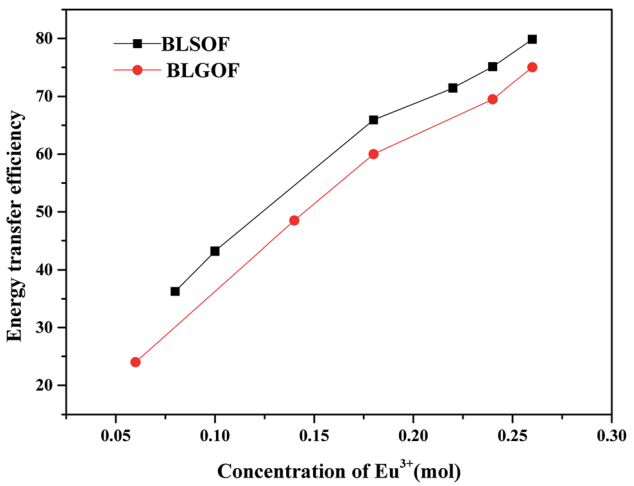

Fig. 10 Comparation of the energy transfer efficiency between BLGOF phosphors and BLSOF phosphors at different Eu^{3+} doping concentrations.

Table 3 CIE coordinate values of BLGOF:0.15Tb^{3+},xEu^{3+} (x = 0, 0.06, 0.14, 0.18, 0.24, and 0.26) and BLGOF:0.15Eu^{3+} at different Eu^{3+} doping concentrations

Number	Formula	CIE value
1	$Ba_2La_{2.85}(GeO_4)_3F$:0.15Tb^{3+}	(0.3684, 0.6093)
2	$Ba_2La_{2.79}(GeO_4)_3F$:0.15Tb^{3+},0.06Eu^{3+}	(0.4807, 0.5055)
3	$Ba_2La_{2.71}(GeO_4)_3F$:0.15Tb^{3+},0.14Eu^{3+}	(0.5689, 0.4239)
4	$Ba_2La_{2.67}(GeO_4)_3F$:0.15Tb^{3+},0.18Eu^{3+}	(0.5957, 0.3990)
5	$Ba_2La_{2.61}(GeO_4)_3F$:0.15Tb^{3+},0.24Eu^{3+}	(0.6158, 0.3804)
6	$Ba_2La_{2.59}(GeO_4)_3F$:0.15Tb^{3+},0.26Eu^{3+}	(0.6258, 0.3711)
7	$Ba_2La_{2.85}(GeO_4)_3F$:0.15Eu^{3+}	(0.6424, 0.3555)

$$R_c \approx 2(3V/4\pi x_c N)^{1/3} \quad (3)$$

For $Ba_2La_3(GeO_4)_3F$ matrix, $N = 10$, $V = 0.666833$ nm^3 (cell volume obtained by structural refinement), the critical concentration of x_c is about 0.301 mol. Therefore, the critical distance of BLGOF:0.15Tb^{3+},xEu^{3+} is 0.7533 nm, so the energy transfer mechanism between Tb^{3+} and Eu^{3+} in BLGOF is electric dipole interaction.

The energy transfer mechanism can be further studied according to the following formula:[41]

$$(I_{S0}/I_S) \propto C^{n/3} \quad (4)$$

I_{S0} is the luminescence intensity of Tb^{3+} when doped with Tb^{3+} only, and I_S is the luminescence intensity of Tb^{3+} when doped with Tb^{3+} and Eu^{3+}. C is the total concentration of Tb^{3+} and Eu^{3+} and n is the constant that can indicate the interaction between Tb^{3+} and Eu^{3+} ($n = 6$, dipole–dipole interaction; $n = 8$, dipole–quadrupole interaction; and $n = 10$, quadrupole–quadrupole interaction).

Linear fitting diagrams of I_{S0}/I_S and $C^{n/3}$ ($n = 6$, 8, or 10) were shown in Fig. 9, respectively. When $n = 10$, the linear fitting is the best. Based on Dexter equation, it can be concluded that the energy transfer mechanism of Tb^{3+}–Eu^{3+} is quadrupole–quadrupole interaction. The energy transfer mechanism is as the same as that of BLSOF:Tb^{3+},Eu^{3+} phosphors.

In order to make the effect of complex anion structure regulation on energy transfer efficiency more intuitive, we compare the energy transfer efficiency of BLGOF with that of BLSOF phosphors, as shown in Fig. 10. Compared with BLSOF, the energy transfer efficiency decreases with the increase of anion radius. This may be due to the effect of complex anions on the environment around rare earth ions, which the radius of complex anions becomes larger and the energy transfer efficiency decreases as a whole.

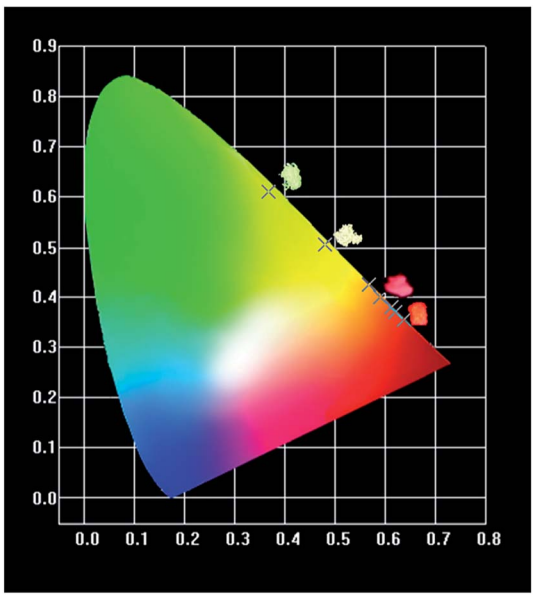

Fig. 11 CIE of BLGOF:0.15Tb^{3+},xEu^{3+} ($x = 0$, 0.06, 0.14, 0.18, 0.24, and 0.26) when excited by 375 nm.

In order to make the application performance of this series of phosphors more intuitive, we calculated the color coordinates of BLGOF:0.15Tb^{3+},xEu^{3+} phosphors excited by 375 nm (Table 3) and labeled them in CIE chromaticity diagram (Fig. 11). At the same time, the digital photos of BLGOF:0.15Tb^{3+}, BLGOF:0.15Tb^{3+},0.06Eu^{3+}, BLGOF:0.15Tb^{3+},0.14Eu^{3+}, BLGOF:0.15Eu^{3+} under 365 nm near ultraviolet light excitation are given in the illustrations of Fig. 11. Thus, by adjusting the doping ratio of Tb^{3+} and Eu^{3+}, the phosphors can

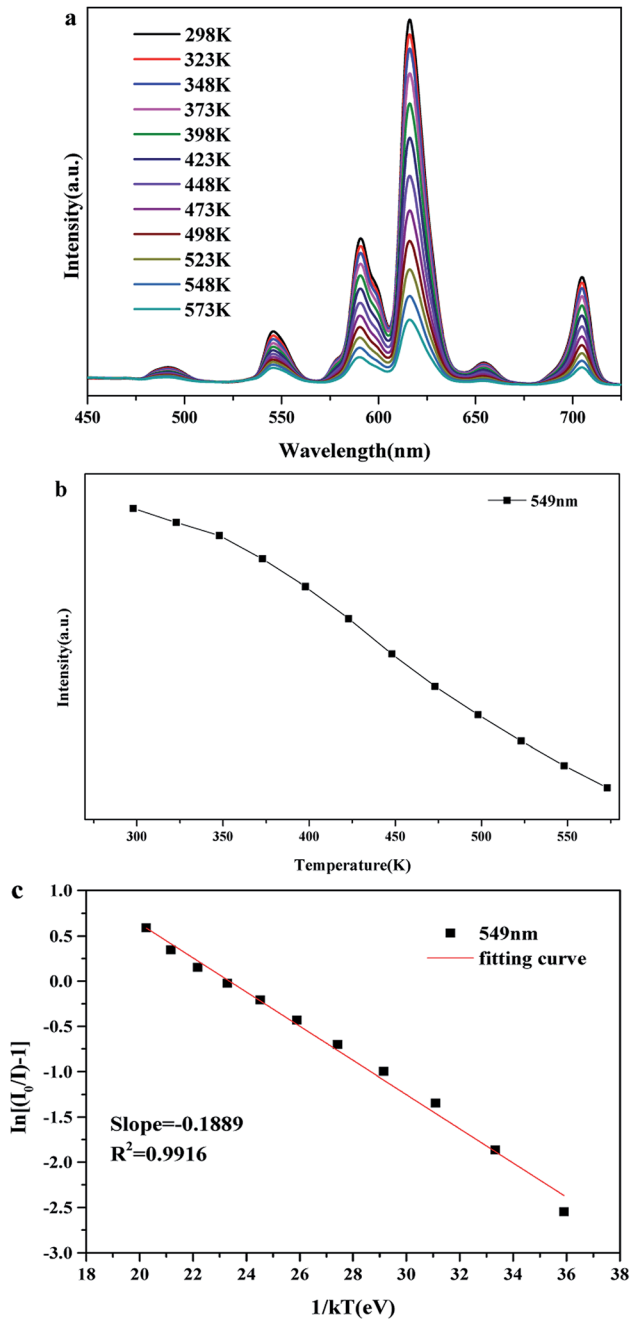

Fig. 12 (a) The luminescence spectra of BLGOF:0.15Tb^{3+},0.24Eu^{3+} at different temperatures (b) the intensity changes of BLGOF:0.15Tb^{3+},0.24Eu^{3+} phosphors 549 nm emission peak at different temperatures (c) $\ln(I_0/I - 1)$ *versus* $1/kT$ for the BLGOF:0.15Tb^{3+},0.24Eu^{3+}.

be changed from green (0.37, 0.61) to yellow, orange-red and red (0.64, 0.36). In conclusion, thanks to energy transfer, the new series of single-phase phosphors BLGOF:0.15Tb^{3+},xEu^{3+} exhibit the advantages of tunable multicolor luminescence under near-ultraviolet (375 nm) excitation.[42,43]

The thermal stability of BLGOF:0.15Tb^{3+},0.24Eu^{3+} phosphor was measured at last.

The temperature-dependent emission spectra and intensity–concentration relationship of Tb^{3+} (549 nm) for BLGOF:0.15Tb^{3+},0.24Eu^{3+} phosphor was shown in Fig. 12(a) and (b). It can be calculated that the luminescence intensity at 423 K remains 67.88% compared to the luminescence intensity at room temperature 298 K. The activation energy was studied in Fig. 12(c) to understand the temperature-dependent thermal quenching behavior according to the following formula:[44]

$$\ln(I_0/I - 1) = \ln A - \Delta E/kT4$$

In which I_0 means the initial emission intensity, I means the emission intensity of different temperatures, A is the coefficient, ΔE means the activation energy, k is the Boltzmann coefficient with a fixed value of 8.629×10^{-5} eV K^{-1} and T is the temperature. Fig. 12(c) shows the linear fit of $\ln(I_0/I - 1)$ *vs.* $1/kT$ for the BLGOF:0.15Tb^{3+} sample and the slope is −0.1889, meaning the activation energy for thermal quenching of Tb^{3+} in BLGOF:0.15Tb^{3+},0.24Eu^{3+} sample is 0.1889 eV.[37] In addition, the quantum efficiency of BLGOF:0.15Tb^{3+},0.24Eu^{3+} sample is 12.36.

4. Conclusions

Generally speaking, a novel multicolor phosphor $Ba_2La_3(GeO_4)_3F$:0.15Tb^{3+},xEu^{3+} has been synthesized by simple solid-state synthesis method. The effects of structure, luminescence behavior and complex anions on Tb^{3+}/Eu^{3+} energy transfer were also studied. The main confusions are as follows: (1) the optimum concentration of Eu^{3+} in BLGOF:0.15Tb^{3+},xEu^{3+} is 0.24 mol. The energy transfer mechanism from Tb^{3+} to Eu^{3+} in BLGOF is quadrupole–quadrupole (q–q), and the complex anion regulation does not change the energy transfer mechanism compared to $Ba_2La_3(SiO_4)_3F$:0.15Tb^{3+},xEu^{3+}. When the doping ratio of Tb^{3+}/Eu^{3+} is different, the color of BLGOF:0.15Tb^{3+},xEu^{3+} phosphors can be changed from green, yellow/orange to red. (2) When $[GeO_4]^{4-}$ was used to replace $[SiO_4]^{4-}$, the cell parameters increased (BLSOF cell volume was 0.620402 (51) nm^3, BLGOF cell volume was 0.666833 (26) nm^3), the overlap area of spectrum became smaller, the energy transfer efficiency decreased. (3) Complex anion regulation has a certain effect on thermal stability. The luminescence intensity of 423 K remains 67.88%, and the thermal stability is good, but less than BLSOF:0.15Tb^{3+},0.22Eu^{3+} at 423 K (85.34%). With the increase of the anion radius of the complex, the luminescence retention rate of 423 K decreases and the activation energy of phosphor increases. All the features acquired above indicate that this phosphor might be a candidate for w-LEDs.

Conflicts of interest

There are no conflicts to declare.

Acknowledgements

This present work is supported by the National Natural Science Foundations of China (Grant no. 51672257, 41672044 and 41172053), and the Fundamental Research Funds for the Central Universities (Grant no. 2652017091 and 2652017370).

References

1 T. M. Tolhurst, T. D. Boyko, P. Pust, N. W. Johnson, W. Schnick and A. Moewes, Investigations of the Electronic Structure and Bandgap of the Next-Generation LED-Phosphor Sr[$LiAl_3N_4$]:Eu^{2+}-Experiment and Calculations, *Adv. Opt. Mater.*, 2015, **3**(4), 546–550.

2 R. Vijayakumar, H. Guo and X. Huang, Energy transfer and color-tunable luminescence properties of Dy^{3+} and Eu^{3+} co-doped $Na_3Sc_2(PO_4)_3$ phosphors for near-UV LED-based warm white LEDs, *Dyes Pigm.*, 2018, **156**, 8–16.

3 X. Gao, J. Yang, M. Zhang, C. G. Liu, H. C. Zhu, D. T. Yan, C. S. Xu and Y. X. Liu, Preparation and Optical Properties of Eu^{2+} Doped $12CaO \cdot 7Al_2O_3$ Blue Emitting Conductive Phosphors, *Chin. J. Lumin.*, 2019, **40**(7), 849–856.

4 M. Runowski, P. Wozny, N. Stopikowska, Q. Guo and S. Lis, Optical Pressure Sensor Based on the Emission and Excitation Band Width (fwhm) and Luminescence Shift of Ce^{3+}-Doped Fluorapatite-High-Pressure Sensing, *ACS Appl. Mater. Interfaces*, 2019, **11**(4), 4131–4138.

5 C.-W. Yeh, Y.-P. Liu, Z. R. Xiao, Y.-K. Wang, S.-F. Hu and R.-S. Liu, Luminescence and density functional theory (DFT) calculation of undoped nitridosilicate phosphors for light-emitting diodes, *J. Mater. Chem.*, 2012, **22**(12), 5828.

6 E. D. Kosten, J. H. Atwater, J. Parsons, A. Polman and H. A. Atwater, Highly efficient GaAs solar cells by limiting light emission angle, *Light: Sci. Appl.*, 2013, **2**, e45.

7 X. Y. Liu, Y. Chen, J. J. Chen, B. B. Lu, S. C. Cui, Q. N. Li and G. H. Chen, Luminescent Properties and Energy Transfer of $Tm^{3+}/Tb^{3+}/Eu^{3+}$ Doped Borate Glass Ceramics, *Chin. J. Lumin.*, 2019, **40**(7), 835–841.

8 H.-H. Fang, F. Wang, S. Adjokatse, N. Zhao, J. Even and M. Antonietta Loi, Photoexcitation dynamics in solution-processed formamidinium lead iodide perovskite thin films for solar cell applications, *Light: Sci. Appl.*, 2016, **5**, e16056.

9 M. Runowski and S. Lis, Preparation and photophysical properties of luminescent nanoparticles based on lanthanide doped fluorides (LaF_3:Ce^{3+}, Gd^{3+}, Eu^{3+}), obtained in the presence of different surfactants, *J. Alloys Compd.*, 2014, **597**, 63–71.

10 Z. Wang, H. Liang, M. Gong and Q. Su, Novel red phosphor of Bi^{3+}, Sm^{3+} co-activated $NaEu(MoO_4)_2$, *Opt. Mater.*, 2007, **29**(7), 896–900.

11 H. Wang, X. Chen, L. Teng, D. Xu, W. Chen, R. Wei, F. Hu, X. Sun and H. Guo, Adjustable emission and energy

transfer process in $BaGd_2O_4$:Bi^{3+},Eu^{3+} phosphors, *J. Lumin.*, 2019, **206**, 185–191.

12 J. Sun, Y. Sun, J. Zeng and H. Du, Luminescence properties and energy transfer investigations of $Sr_3Gd(PO_4)_3$:Ce^{3+},Tb^{3+} phosphors, *J. Phys. Chem. Solids*, 2013, **74**(7), 1007–1011.

13 J. Xiong, Q. Meng and W. Sun, Luminescent properties and energy transfer mechanism from Tb^{3+} to Eu^{3+} in $CaMoO_4$:Tb^{3+},Eu^{3+} phosphors, *J. Rare Earths*, 2016, **34**(3), 251–258.

14 M. Shang, D. Geng, D. Yang, X. Kang, Y. Zhang and J. Lin, Luminescence and energy transfer properties of $Ca_2Ba_3(PO_4)_3Cl$ and $Ca_2Ba_3(PO_4)_3Cl$:A (A = Eu^{2+}/Ce^{3+}/Dy^{3+}/Tb^{3+}) under UV and low-voltage electron beam excitation, *Inorg. Chem.*, 2013, **52**(6), 3102–3112.

15 B. Szpikowska-Sroka, N. Pawlik, M. Bańczyk and W. A. Pisarski, Tb^{3+}/Eu^{3+} co-doped silica xerogels prepared via low-temperature sol-gel method and their luminescence properties, *Mater. Lett.*, 2019, **235**, 101–103.

16 J. Y. Sun, D. P. Cui, B. Xue, G. C. Sun and H. Y. Du, Luminescence Properties and Energy Transfer from Eu^{2+} to Tb^{3+} in $Sr_5(PO_4)_3F$ Phosphor, *Adv. Mater. Res.*, 2013, **683**, 199–202.

17 P. S. Thakre, S. C. Gedam, S. J. Dhoble and R. G. Atram, Luminescence investigations on sulfate apatite $Na_6(SO_4)_2FCl$:RE (RE = Dy, Ce or Eu) phosphors, *J. Lumin.*, 2011, **131**(12), 2683–2689.

18 T. Wanjun and Z. Fen, A Single-Phase Emission-Tunable $Ca_5(PO_4)_3F$:Eu^{2+},Mn^{2+} Phosphor with Efficient Energy Transfer for White LEDs, *Eur. J. Inorg. Chem.*, 2014, **2014**(21), 3387–3392.

19 S. Yan, Y. Jin, D. Pan, G. Xiang, X. Luo and Y. Yang, $Sr_4Y_6(AlO_4)_x(SiO_4)_{6-x}O_\delta$:$Eu^{2+}$: a novel apatite structure blue-green emitting phosphor, *Ceram. Int.*, 2018, **44**(16), 19900–19906.

20 *Bruker AXS TOPAS V4: General profile and structure analysis software for powder diffraction data – User's Manual*, Bruker AXS, Karlsruhe, Germany, 2008.

21 X. H. Gong, Y. F. Lin, Y. J. Chen, Z. X. Huang, Y. D. Huang and Z. D. Luo, Syntheses, Structure, and Characterization of Crystal $La_6Ba_4(SiO_4)_6F_2$, a Promising Laser Host, *Chem. Mater.*, 2005, **17**, 1135–1138.

22 M. Runowski, S. Goderski, J. Paczesny, M. Księżopolska-Gocalska, A. Ekner-Grzyb, T. Grzyb, J. D. Rybka, M. Giersig and S. Lis, Preparation of Biocompatible, Luminescent-Plasmonic Core/Shell Nanomaterials Based on Lanthanide and Gold Nanoparticles Exhibiting SERS Effects, *J. Phys. Chem. C*, 2016, **120**(41), 23788–23798.

23 J. Zhao, L. Kang, Z. Lin and R. K. Li, $Ba_{1.31}Sr_{3.69}(BO_3)_3Cl$: a new structure type in the $M_5(BO_3)_3Cl$ (M = bivalent cation) system, *J. Alloys Compd.*, 2017, **699**, 136–143.

24 J. Yan, L. Ning, Y. Huang, C. Liu, D. Hou, B. Zhang, Y. Huang, Y. Tao and H. Liang, Luminescence and electronic properties of $Ba_2MgSi_2O_7$:Eu^{2+}: a combined experimental and hybrid density functional theory study, *J. Mater. Chem. C*, 2014, **2**(39), 8328–8332.

25 L. Zhu, Z. Huang, M. S. Molokeev, X. Min, Y. Liu, M. Fang and X. Wu, Influence of cation substitution on the crystal structure and luminescent properties in apatite structural $Ba_{4.97-x}Sr_x(PO_4)_3Cl$:0.03$Eu^{2+}$ phosphors, *Chem. Phys. Lett.*, 2016, **658**, 248–253.

26 X. Zhang, H. Zou, C. Xu, Z. An, R. Dong, K. Zheng, Y. Sheng and Y. Song, Energy transfer and luminescence properties of Dy^{3+}/Eu^{3+} doped silicoaluminate phosphors, *Opt. Mater.*, 2019, **89**, 512–520.

27 Y. Zhang, L. Mei, H. Liu, D. Yang, L. Liao and Z. Huang, Dysprosium doped novel apatite-type white-emitting phosphor $Ca_9La(PO_4)_5(GeO_4)F_2$ with satisfactory thermal properties for n-UV w-LEDs, *Dyes Pigm.*, 2017, **139**, 180–186.

28 L. Zhang, H. Pan, H. Liu, B. Zhang, L. Jin, M. Zhu and W. Yang, Theoretical spectra identification and fluorescent properties of reddish orange Sm-doped $BaTiO_3$ phosphors, *J. Alloys Compd.*, 2015, **643**, 247–252.

29 X. Zhang and M. Gong, Eu^{2+}-doped halo-phosphate/borate phosphors for color temperature tunable near UV-based white light-emitting diodes, *Mater. Chem. Phys.*, 2010, **124**(2–3), 1243–1247.

30 R. Zhang, B. Wang, P. Zhou, X. Wu, X. Huang and B. Wang, A novel Ce^{3+}:$Y_3Al_5O_{12}$ and Eu^{2+}:$Sr_2Si_5N_8$ dual phosphors-in-glass thick film for warm white LED, *Mater. Lett.*, 2018, **221**, 31–34.

31 X. Zeng, S.-J. Im, S.-H. Jang, Y.-M. Kim, H.-B. Park, S.-H. Son, H. Hatanaka, G.-Y. Kim and S.-G. Kim, Luminescent properties of (Y,Gd)BO_3:Bi^{3+},RE^{3+} (RE = Eu, Tb) phosphor under VUV/UV excitation, *J. Lumin.*, 2006, **121**(1), 1–6.

32 X. Zhu and Z. Zhou, Photoluminescence and energy transfer mechanism of a novel tunable color phosphor Na_2MgSiO_4:Tb^{3+},Eu^{3+}, *J. Lumin.*, 2017, **188**, 589–594.

33 H. Liu, Y. Luo, Z. Mao, L. Liao and Z. Xia, A novel single-composition trichromatic white-emitting $Sr_{3.5}Y_{6.5}O_2(PO_4)_{1.5}(SiO_4)_{4.5}$:$Ce^{3+}$/$Tb^{3+}$/$Mn^{2+}$ phosphor: synthesis, luminescent properties and applications for white LEDs, *J. Mater. Chem. C*, 2014, **2**(9), 1619.

34 Q. Zhang, J. Wang, R. Yu, M. Zhang and Q. Su, Luminescence Properties of Eu^{2+} Ions in $Sr_5(BO_3)_3Cl$, *Electrochem. Solid-State Lett.*, 2008, **11**(12), H335.

35 J. Xie, L. Mei, L. Liao, M. Guan and H. Liu, Synthesis and up-conversion luminescence properties of Ho^{3+}, Yb^{3+} co-doped $BaLa_2ZnO_5$, *J. Phys. Chem. Solids*, 2015, **83**, 152–156.

36 Y. Zhang, L. Mei, H. Liu, J.-C. Chang, W.-R. Liu and Z. Huang, Thermal-stable and high-efficient orange-red emitting orthosilicate phosphors $LiGd_9(SiO_4)_6O_2$:Mn^{2+} for n-UV-pumped w-LEDs, *Mater. Chem. Phys.*, 2019, **228**, 215–220.

37 M. Shang, G. Li, D. Geng, D. Yang, X. Kang, Y. Zhang, H. Lian and J. Lin, Blue Emitting $Ca_8La_2(PO_4)_6O_2$:Ce^{3+}/Eu^{2+} Phosphors with High Color Purity and Brightness for White LED: Soft-Chemical Synthesis, Luminescence, and Energy Transfer Properties, *J. Phys. Chem. C*, 2012, **116**(18), 10222–10231.

38 C. Zeng, H. Liu, Y. Hu, L. Liao and L. Mei, Color-tunable properties and energy transfer in $Ba_3GdNa(PO_4)_3F$:Eu^{2+},Tb^{3+} phosphor pumped for n-UV w-LEDs, *Opt. Laser Technol.*, 2015, **74**, 6–10.

39 J. Zhao, C. Guo, T. Li, X. Su, N. Zhang and J. Chen, Synthesis, electronic structure and photoluminescence properties of $Ba_2BiV_3O_{11}$:Eu^{3+} red phosphor, *Dyes Pigm.*, 2016, **132**, 159–166.

40 X. Zhou, W. Geng, J. Ding, Y. Wang and Y. Wang, Structure, bandgap, photoluminescence evolution and thermal stability improved of Sr replacement apatite phosphors $Ca_{10-x}Sr_x(PO_4)_6F_2$:Eu^{2+} ($x = 4$, 6, 8), *Dyes Pigm.*, 2018, **152**, 75–84.

41 Y. Zhang, L. Mei, H. Liu, X. Ma, Z. Huang and L. Liao, Photoluminescence properties and energy transfer behavior of Eu^{2+}/Tb^{3+} co-doped $Ba_3Sc(PO_4)_3$ phosphors, *Ceram. Int.*, 2015, **41**(10), 14698–14702.

42 X. Zhang, J. Zhang, J. Huang, X. Tang and M. Gong, Synthesis and luminescence of Eu^{2+}-doped alkaline-earth apatites for application in white LED, *J. Lumin.*, 2010, **130**(4), 554–559.

43 Z. Zhang, O. M. ten Kate, A. C. A. Delsing, M. J. H. Stevens, J. Zhao, P. H. L. Notten, P. Dorenbos and H. T. Hintzen, Photoluminescence properties of Yb^{2+} in $CaAlSiN_3$ as a novel red-emitting phosphor for white LEDs, *J. Mater. Chem.*, 2012, **22**(45), 23871.

44 X. Zhang, J. Zhang and M. Gong, Synthesis and luminescent properties of UV-excited thermal stable red-emitting phosphor $Ba_3Lu(PO_4)_3$:Eu^{3+} for NUV LED, *Opt. Mater.*, 2014, **36**(4), 850–853.